Met. Mater. Int., Vol. 16, No. 3 (2010), pp. 501~506
doi: 10.1007/s12540-010-0601-y Published 26 June 2010

Effect of Refractory Properties on Initial Bubble Formation in Continuous-Casting Nozzles

Go-Gi Lee[1], Brian G. Thomas[2], and Seon-Hyo Kim[3,*]

[1] Research Institute of Industrial Science and Technology (RIST),
San32, Hyojadong, Pohang-si, Gyeongbuk 790-784, Korea
[2] Department of Mechanical Science and Engineering,
University of Illinois at Urbana-Champaign, Urbana, IL 61801, USA
[3] Department of Material Science and Engineering, Pohang University of Science and Technology,
San31, Hyoja-dong, Pohang-si, Gyeongbuk 790-784, Korea

(received date: 14 August 2009 / accepted date: 5 November 2009)

A water model has been applied to investigate initial bubble behavior using specially-coated samples of porous MgO refractory to simulate the high-contact angle of steel-argon refractory systems with different permeabilities. Air is injected through the porous refractory and travels through many inter-connected pores to exit the surface through "active sites". An active site is a pore where bubbles exit from the surface of the porous refractory. The effect of refractory properties has been investigated in both stagnant and downward-flowing water. The number of active sites increases with increasing gas injection flow rate, permeability, and velocity of the downward-flowing water, and lower contact angle.

Keywords: porous refractory, permeability, bubble, nozzle, continuous casting

1. INTRODUCTION

Argon gas is injected into downward-flowing liquid steel through the upper tundish nozzle (UTN), which connects the tundish bottom and slide gate system. The fluid flow in the submerged entry nozzle (SEN) is highly turbulent, and depends greatly on the amount and size of injected gas. Furthermore, the flow pattern in the mold is strongly affected by the fluid flow at the nozzle ports. Gas bubbles injected through the UTN could penetrate deep into the mold and become entrapped in the solidifying steel shell [1], where they cause blisters and other costly defects [2,3]. Knowledge and interpretation of the size of bubbles forming in the nozzle, therefore, are essential for the prediction and understanding of multiphase fluid flow behavior and related defects in the continuous casting process.

Due to high operating temperature, it is difficult and expensive to directly investigate bubble formation in continuous steel casters [4]. Physical water model experiments with transparent plastic walls, therefore, have been employed to gain insight into single-phase fluid flow in steel casting processes [5-10]. For these models, Froude dimensionless number similarity is usually applied due to the nearly equal kinematic viscosities of molten steel and water.

Extensive studies [11-16] of bubble formation have been performed on aqueous systems both experimentally and theoretically. Recently, Wang *et al*. [17] used water models to study air-bubble formation from gas injected through a porous refractory into an acrylic nozzle with flowing water. The wettability was reduced by waxing the walls, which caused the gas to form large pockets that travel along the wall and break up into many uneven-sized bubbles. With an unwaxed surface, relatively uniform-sized bubbles were formed and detached from the wall to join the liquid flow. Although most previous studies focused on bubble formation from an upward-facing orifice or nozzle, some authors [14,18] have observed that bubbles formed from a horizontal orifice behaved in a highly similar manner to that in stagnant flow. Bai and Thomas [15] developed a correlation to predict average bubble size in both water model experiments and steel–argon systems, as a function of downward water velocity and gas flow rate injected horizontally through drilled holes. There has been no reported study, however, on the effects of refractory properties and major processing parameters on bubble formation in the nozzle.

The present study was conducted to quantify bubble size and distribution during gas injection into downward flowing

*Corresponding author: seonhyo@postech.ac.kr

water through realistic porous refractory materials. The effects of liquid velocity, gas flow rate, and contact angle on the mean bubble size, distribution, and the number of active sites on the porous refractory surface are evaluated in order to clarify the bubble behavior in a steel caster mold.

2. EXPERIMENTAL PROCEDURE

Figure 1 shows a schematic of the water model apparatus. Water flow in liter per minute (LPM) exits from the tundish bottom through a UTN nozzle. Air is injected through a porous refractory sample (14 mm wide × 44 mm long × 17 mm deep) centered in a representative portion of the nozzle wall. The water flow rate is controlled by the slide gate system to achieve 20 LPM to 45 LPM, which corresponds to average downward water velocities, V_l, inside the nozzle ranging from 0.68 m/s to 1.58 m/s, considering the square 22 mm × 22 mm nozzle cross-sectional area. The square nozzle shape enables clear observation of the initial bubble behavior inside the nozzle without distortion from refraction.

The porous MgO refractory specimens were manufactured with various permeabilities, P_{erm}, as given in Table 1. The wettability between molten steel and the porous refractory has a great influence on bubble formation in the nozzle [19,20]. To achieve the same poor wettability (high contact angle) between water and porous refractory simulating the actual system, the surface of the porous MgO refractory was specially treated to lower its wettability. With this method, an active layer was first formed on the surface of a porous refractory by oxidizing the surface with O_2 plasma. The refractory was then immersed in Silane solution, (1H, 1H, 2H, 2H Perfluoro-Dodecyltrichlorosilane), which reacts to form a thin siloxane layer (R_2SiO, where R is a hydrogen atom or a hydrocarbon group), as illustrated in Fig. 2 [21]. In the adsorption process, the water layer on the MgO attracts the surfactants. The hydrophilic head groups of alkylsilanes (R_nSiX_{4-n}, where X is a hydrolysable leaving group, and R is an alkyl chain or phenyl moiety with an organic functional group) are gradually absorbed onto the water layer. Following the adsorption, the head groups are hydrolyzed into sil-

Table 1. Properties of porous MgO refractory bricks

	Brick 1	Brick 2	Brick 3
Fired B. D. (g/cc)	2.9	2.9	2.8
Porosity (%)	16.2	17.6	17.6
Modulus of rupture (MPa)	7.48	7.72	10.1
Average pore perimeter (um)	252	302	306
Average pore area (um^2)	3097	4928	4949
Permeability (nPm)	7.52	16.32	26.12

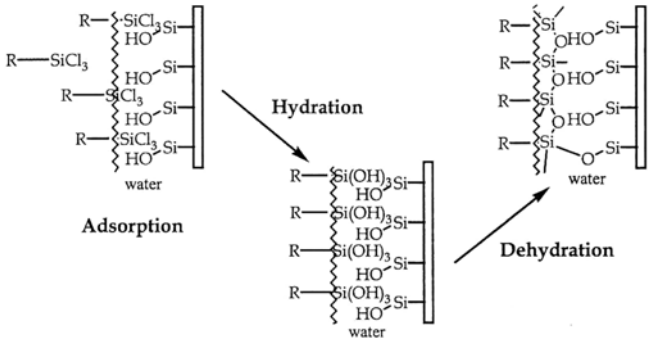

Fig. 2. Mechanism of siloxane layer formation [21].

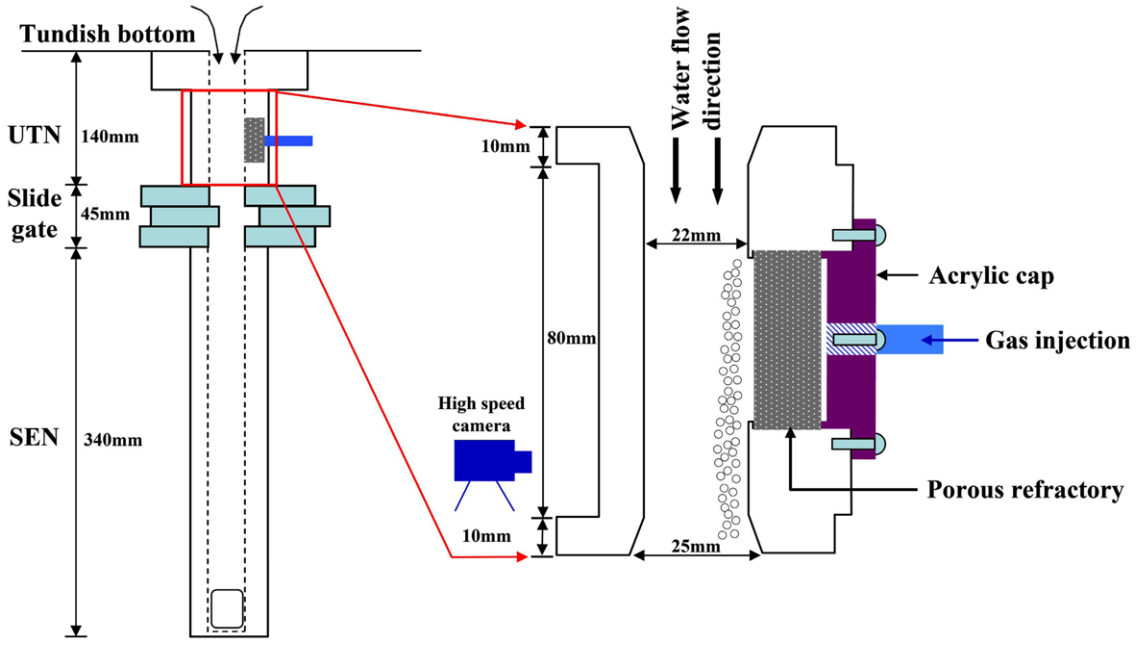

Fig. 1. Gas injection through porous MgO refractory UTN.

Table 2. Relationship of liquid flow rate between water model and steel caster

Water flow rate (Q_W, SLPM)	28.2	32.5	36.8
Liquid velocity in nozzle (U_W=U_S, m/s)	0.96	1.10	1.25
Steel throughput (Q_S, m^3/min)	0.25	0.29	0.33
Casting speed (m/min, 230 mm thick × 1500 mm wide)	0.74	0.85	0.96

anols (-nSiOH) and the siloxane bond is finally formed by elimination of H_2O molecules between silanols. The driving force for self assembly is the *in-situ* formation of polysiloxane, which is connected to a surface silanol group via Si-O-Si bonds.

The gas flow rate, Q_g, was adjusted to 0.1 to 1.0 standard liter per minute (SLPM), in order to achieve average injection velocities (flow rates per unit area of refractory surface) of 0.016 SLPM/cm^2 to 0.162 SLPM/cm^2. The gas is injected into a tube inserted in the back side of the porous refractory specimen, spreads through the many inter-connected pores, and finally leaves the refractory surface. The initial bubble formation before entering slide gate system was recorded by a high speed camera at 4000 frames per second, and then studied by inspecting the video images frame by frame. Representative recorded-images are shown in Fig. 3 for three water velocities and gas flow rates. Each pore where bubbles emerge from the porous refractory surface is termed an "active site". In addition to counting the active sites, the bubble size and distribution were also determined through direct measurements from individual video images.

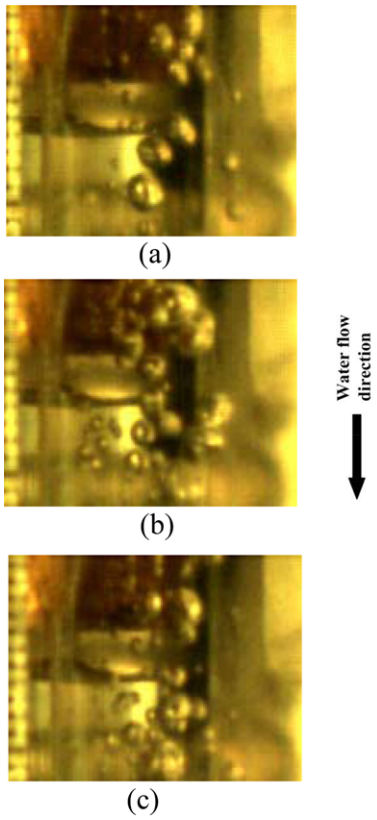

Fig. 3. Photos of water-model experiments with various water velocity V_l and gas velocity V_g in nozzle with 7.52 nPm permeability: (a) V_l =0.97 m/s; V_g=0.0027 m/s (b) V_l=0.97 m/s; V_g=0.0081 m/s, and (c) V_l=1.27 m/s; V_g=0.0081 m/s.

3. RESULTS AND DISCUSSION

3.1. Active site measurement

Water model experiments were first performed in stagnant water by immersing the UTN into a water bath. The results were compared with observations in a nozzle with downward-flowing water at a mean velocity, U, of 1.25 m/s. For a typical steel casting nozzle of 75 mm diameter, (area = 0.00442 m^2) this water velocity corresponds with a steel flow rate Q_s of 0.33 m^3/s, or a casting speed V_C of 0.96 m/min for a 230 mm × 1500 mm slab section, as follows:

$$V_C = \left(\frac{Q_S}{\text{cross-section area of slab}} \right) \quad (1)$$

Figure 4 shows the number of active sites of bubbles evolving from the surface pores of the porous refractory in both stagnant and downward-flowing water systems without surface treatment. Each point for downward-flowing water in Fig. 4 represents the mean of five replicate tests performed under identical conditions. The number of active sites consistently increases with increasing gas injection flow rate. Figure 3 clearly shows the effect of downward-flowing velocity increasing the number of active sites, relative to stagnant flow. Drag from the downward-flowing water along the refractory surface acts to shear the bubbles into

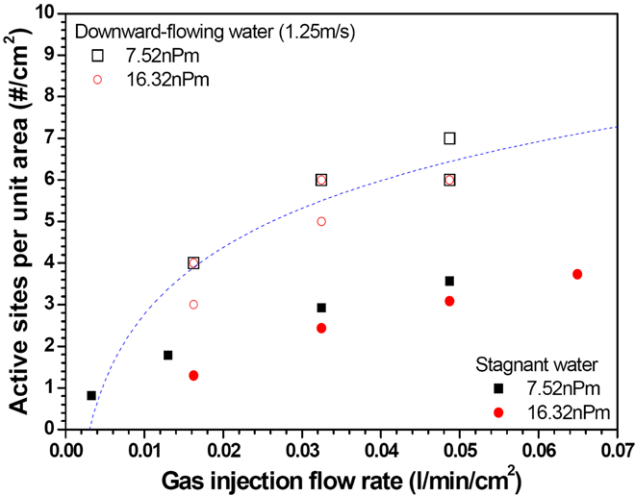

Fig. 4. Active sites in both stagnant and downward-flowing water (uncoated refractory).

the water stream before they grow to the mature sizes found in stagnant flow. This drag force produces a smaller bubble size induced by downward flow, which corresponds with observations by Bai [15]. Fewer active sites form due to the local dynamic pressure drop. The effect of refractory permeability is not clear in downward-flowing water whereas it is known that decreasing permeability increases active sites in stagnant flow.

3.2. Bubble size and distributions

The water model measurements show that both the mean bubble size and the variation of its distribution increase with increasing gas injection flow rate, as well as with decreasing water velocity, as shown in Fig. 5. Decreasing the water velocity below a critical minimum level (such as that found in recirculation regions beneath the slide gate) facilitates the formation of very large bubbles [15]. The periodic release of such large gas pockets might result in significant level fluctuations in the mold, leading to the entrapment of molten mold flux and surface defects associated with an unstable meniscus.

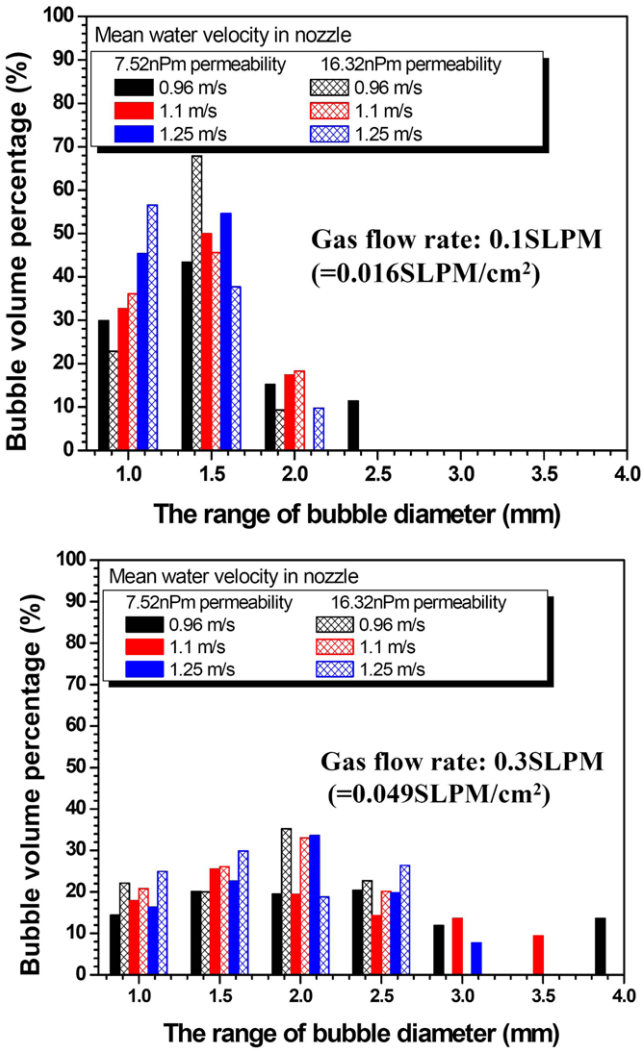

Fig. 5. Bubble size distribution with different water velocity and gas flow rate (6.2 cm^2 surface area of uncoated refractory sample).

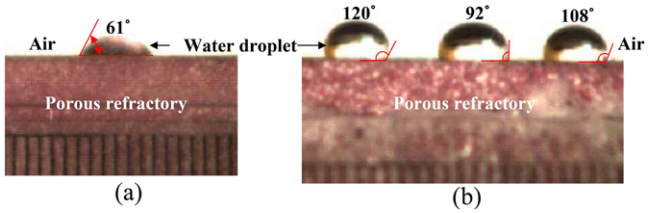

Fig. 6. Contact angle (a) before surface coating, (b) after surface coating.

3.3. Effect of wettability on active sites

Figure 6 shows the change of contact angle after coating the surface of the porous refractory from 61 deg (uncoated) to ~107 deg (coated). Figure 7 shows the rough surface of the coated refractory using optical microscopy and a scanning electron microscope (SEM) for image analysis. The coating layer in Fig. 7(b) appears to be ~40 μm thick, which is smaller than the measured average pore diameter of 80 μm. The elements Si and Cl were detected as the main couplers with surface oxygen through electron dispersive X-ray spectroscopy (EDXS). This coating layer is strong enough to persist throughout the water experiments, as seen in Fig. 7(c).

Figure 8 shows the sharp decrease in the number of active sites with higher gas flow rates after coating the refractory surface. The number of active sites with surface coating decreases, under the same gas flow rate per site, which causes a lower frequency of bubble formation. This finding is consistent with the larger bubble size anticipated with the low wettability of real molten metal systems. The number of active sites also decreases with decreasing permeability.

From a regression of the surface coating experimental results, the following empirical equation was derived to predict the active sites.

$$\text{Active sites per unit area}\left(\#/\text{cm}^2\right) = 7 \times \frac{Q_g^{0.2635} \times U^{0.85} \times P_{erm}^{0.3308}}{Radians(\theta)} \quad (2)$$

Figure 9 compares the measured active sites per unit area with estimates obtained using this equation.

The mean bubble size and its distribution (error bars) with the coated refractory was measured as shown in Fig. 10. Bubble size is larger with the coated refractory (compared with the uncoated case in Fig. 5). Bubble size of the coated refractory also increases with decreasing permeability and with increasing flow rate, due to the corresponding decrease in the number of active sites. Bubble flow changed from bubbly flow to a continuous gas curtain with an increase of the gas flow rate above a critical limit of about 0.2 SLPM/

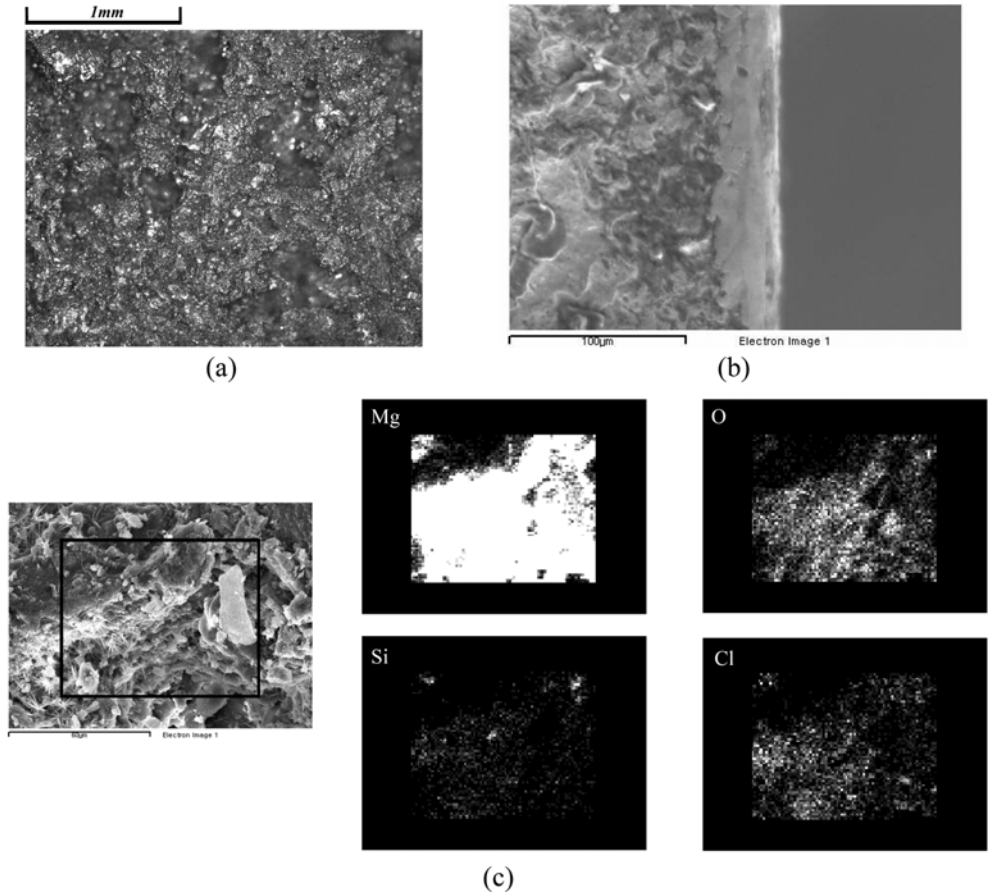

Fig. 7. Close-up of surface coating with 7.52 nPm permeability showing (a) pores (top view), (b) surface coating thickness (side view), and (c) evidence of surface coating material after water experiments.

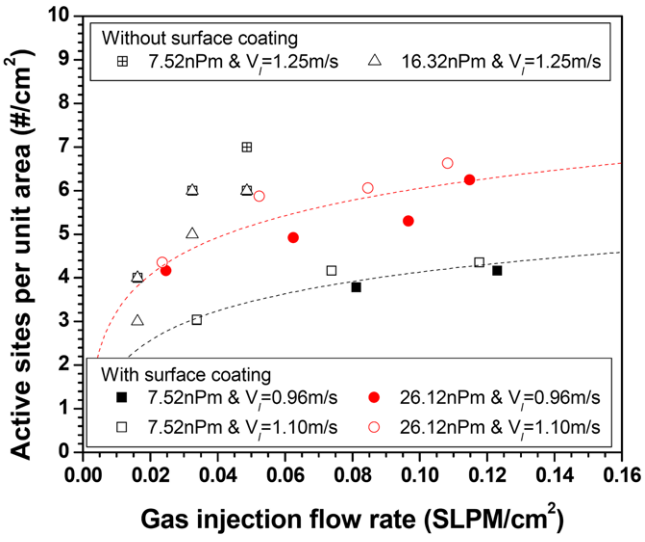

Fig. 8. Comparison of active sites with and without surface coating of porous refractory in downward-flowing water.

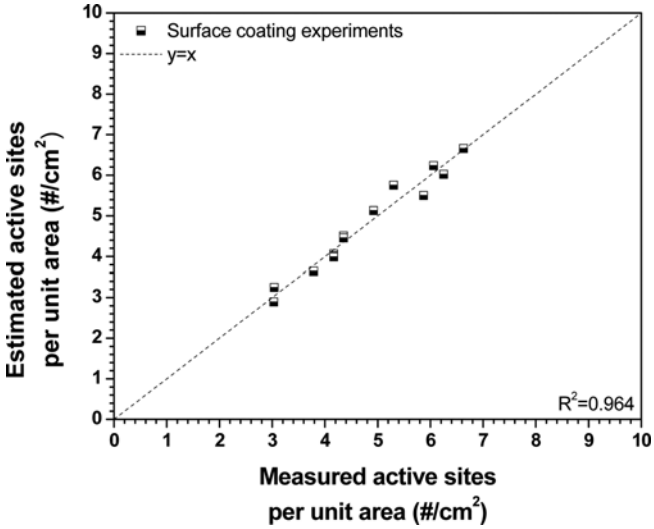

Fig. 9. Comparison of the measured and estimated active sites with surface coating of porous refractory in downward-flowing water.

cm^2. Consequently, the bubbles showed a greater tendency to spread into a gas pocket and curtain over the refractory wall. The present work lends new insight into the design of future water models. In future work, systematic investigation of the phenomena of initial bubble formation and behavior in the nozzle and mold is needed.

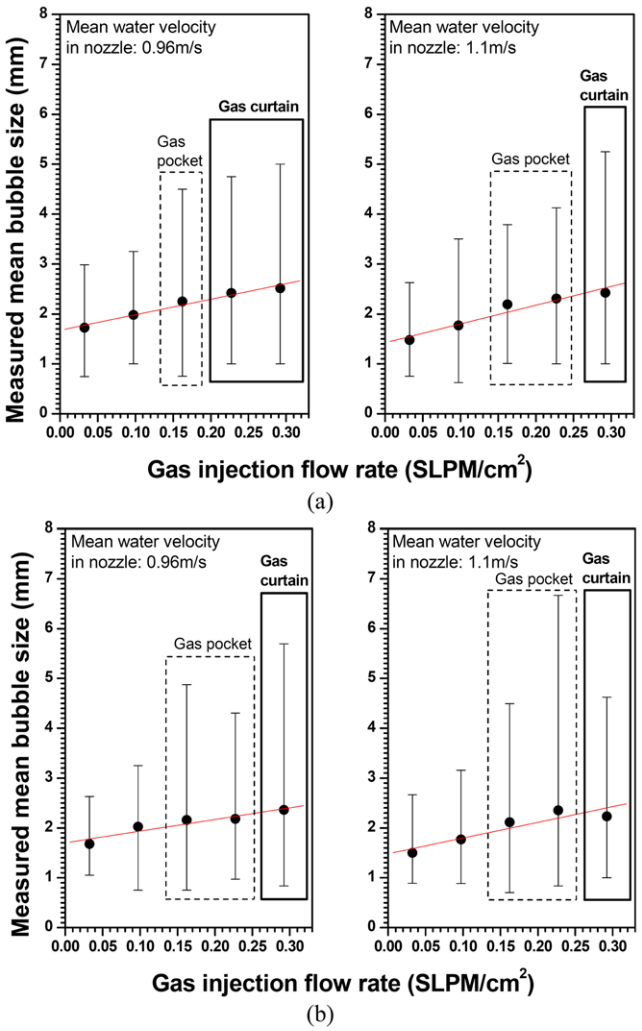

Fig. 10. Bubble size distribution using coated refractory with different permeabilities: (a) 7.52 nPm and (b) 26.12 nPm.

4. CONCLUSIONS

The initial stages of bubble formation injecting gas through porous MgO refractory into a downward turbulent water flow has been studied with water model experiments. The active sites, that is, the actual site where the bubble exits the surface of porous MgO refractory, were used to investigate the effects of refractory properties on bubble formation. The effects of downward-flowing water velocity, gas injection flow rate, and surface contact angle on the bubble size, distribution, and the active sites were quantified. These effects provide new insight into multiphase water model experiments to aid in the design of future water models. Nevertheless, further work is needed to investigate initial bubble formation and bubble behavior in nozzles and molds with higher contact angle.

ACKNOWLEDGMENTS

The authors are grateful to Technology Innovation Center for Metals & Materials at POSTECH for use of their facilities, and also thank to Continuous Casting Consortium at the University of Illinois at Urbana-Champaign for support of this project, especially Rob Nunnington and LWB Refractories for supplying samples.

REFERENCES

1. Y. Shirota, *143rd-144th Nishiyama Memorial Seminar*, ISIJ, Tokyo (1992).
2. J. Herbertson, Q. L. He, P. J. Flint, and R. B. Mahapatra, *Steelmaking Conf. Proc.*, p. 171-185, ISS, Warrendale, Washington, D.C., PA (1991).
3. K. C. Cho, Y. M. Koo, and J. K. Park, *J. Kor. Inst. Met & Mater.* **46**, 329 (2008).
4. B. G. Thomas, Q. Yuan, S. Sivaramakrishnan, T. Shi, S. P. Vanka, and M. B. Assar, *ISIJ Int.* **41**, 1262 (2001).
5. R. Sobolewski and D. J. Hurtuk, *2nd Process Technology Conf. Proc.*, p. 160-165, Iron and Steel Society, Warrendale, PA (1982).
6. B. G. Thomas, X. Huang, and R. C. Sussman, *Metall. Trans. B* **25B**, 527 (1994).
7. D. Gupta and A. K. Lahiri, *Metall. Mater. Trans. B* **27**, 757 (1996).
8. D. Gupta, S. Chakraborty, and A. K. Lahiri, *ISIJ Int.* **37**, 654 (1997).
9. S. Sivaramakrishnan, B. G. Thomas, and S. P. Vanka, *Materials Processing in the Computer Age* (eds., V. Voller and H. Henein), p. 189-198, TMS, Warrendale, PA (2000).
10. M. B. Assar, P. H. Dauby, and G. D. Lawson, *Steelmaking Conf. Proc.*, p. 397-411, ISS, Warrendale, Pittsburgh, PA (2000).
11. H. Tsuge, *Encyclopedia of Fluid Mechnics* (ed., G. P. Co), p. 191-232, Houston, TX (1986).
12. N. Rabiger and A. Vogelpohl, *Encyclopedia of Fluid Mechnics* (ed., G. P. Co), p. 58-88, Houston, TX (1986).
13. R. Clift, J. R. Grace, and M. E. Weber, *Bubbles, Drops and Particles*, Academics Press, INC, New York (1978).
14. R. Kumar and N. R. Kuloor, *Advances in Chemical Engineering* (ed., A. Press), p. 255-368, New York (1970).
15. H. Bai and B. G. Thomas, *Metall. Mater. Trans. B* **32**, 1143 (2001).
16. L. F. Zhang, S. B. Yang, K. K. Cai, J. Y. Li, X. G. Wan, and B. G. Thomas, *Metall. Mater. Trans. B* **38**, 63 (2007).
17. Z. Wang, K. Mukai, and D. Izu, *ISIJ Int.* **39**, 154 (1999).
18. G. A. Irons and R. I. L. Guthrie, *Met. Mater. Trans. B* **9**, 101 (1978).
19. Z. Wang, K. Mukai, K. Yamaguchi, and I. J. Lee, *CAMP-ISIJ* **11**, 24 (1998).
20. Z. Wang, K. Mukai, K. Matsuoka, and I. J. Lee, *CAMP-ISIJ* **10**, 68 (1997).
21. J. Bryzek, K. Petersen, and W. McCulley, *IEEE Spectrum* **31**, 20 (1994).